

# Ryanodine receptor cluster fragmentation and redistribution in persistent atrial fibrillation enhance calcium release

Niall Macquaide<sup>1,2,3</sup>, Hoang-Trong Minh Tuan<sup>4</sup>, Jun-ichi Hotta<sup>5</sup>, Wouter Sempels<sup>5</sup>, Ilse Lenaerts<sup>1</sup>, Patricia Holemans<sup>1</sup>, Johan Hofkens<sup>5</sup>, M. Saleet Jafri<sup>6</sup>, Rik Willems<sup>1,2,3</sup>, and Karin R. Sipido<sup>1\*</sup>

<sup>1</sup>Department of Cardiovascular Sciences, Experimental Cardiology, KU Leuven, Campus Gasthuisberg O/N 7th Floor, Herestraat 49, B-3000 Leuven, Belgium; <sup>2</sup>Department of Molecular Neuroscience, George Mason University, Fairfax, VA, USA; <sup>3</sup>Institute of Cardiovascular Sciences, University of Glasgow, Glasgow, UK; <sup>4</sup>School of Systems Biology, George Mason University, Manassas, VA, USA; <sup>5</sup>Laboratory of Photochemistry and Spectroscopy, Department of Chemistry, KU Leuven, Leuven, Belgium; and <sup>6</sup>Department of Cardiology, University Hospitals Leuven, Leuven, Belgium

Received 6 February 2015; revised 5 October 2015; accepted 6 October 2015; online publish-ahead-of-print 21 October 2015

Time for primary review: 27 days

This manuscript was handled by a Consulting Editor.

## Aims

In atrial fibrillation (AF), abnormalities in Ca<sup>2+</sup> release contribute to arrhythmia generation and contractile dysfunction. We explore whether ryanodine receptor (RyR) cluster ultrastructure is altered and is associated with functional abnormalities in AF.

## Methods and results

Using high-resolution confocal microscopy (STED), we examined RyR cluster morphology in fixed atrial myocytes from sheep with persistent AF ( $N = 6$ ) and control (Ctrl;  $N = 6$ ) animals. RyR clusters on average contained 15 contiguous RyRs; this did not differ between AF and Ctrl. However, the distance between clusters was significantly reduced in AF ( $288 \pm 12$  vs.  $376 \pm 17$  nm). When RyR clusters were grouped into Ca<sup>2+</sup> release units (CRUs), i.e. clusters separated by  $< 150$  nm, CRUs in AF had more clusters ( $3.43 \pm 0.10$  vs.  $2.95 \pm 0.02$  in Ctrl), which were more dispersed. Furthermore, in AF cells, more RyR clusters were found between Z lines. In parallel experiments, Ca<sup>2+</sup> sparks were monitored in live permeabilized myocytes. In AF, myocytes had  $> 50\%$  higher spark frequency with increased spark time to peak (TTP) and duration, and a higher incidence of macrosparks. A computational model of the CRU was used to simulate the morphological alterations observed in AF cells. Increasing cluster fragmentation to the level observed in AF cells caused the observed changes, i.e. higher spark frequency, increased TTP and duration; RyR clusters dispersed between Z-lines increased the occurrence of macrosparks.

## Conclusion

In persistent AF, ultrastructural reorganization of RyR clusters within CRUs is associated with overactive Ca<sup>2+</sup> release, increasing the likelihood of propagating Ca<sup>2+</sup> release.

## Keywords

Atrial fibrillation • Atrial myocytes • Sarcoplasmic reticulum • Ryanodine receptor • Super-resolution microscopy

## 1. Introduction

Atrial fibrillation (AF) is the most common cardiac arrhythmia.<sup>1</sup> The resultant loss of atrial contraction leads to atrial thrombi; embolization and stroke are major causes of morbidity and mortality. In persistent AF, antiarrhythmic drug and catheter ablation therapies are less effective.<sup>2</sup> Further understanding of the cellular processes involved in the generation and maintenance of AF may help to identify novel targets for antiarrhythmic treatment.<sup>3</sup>

Recently, evidence has emerged for a major role of dysregulation of ryanodine receptor (RyR) function and Ca<sup>2+</sup> release from the sarcoplasmic reticulum (SR). An increase in RyR activity, attributed to an up-regulation of CaMKII, was reported in patients with persistent AF.<sup>4,5</sup> This may lead to an increased propensity for spontaneous Ca<sup>2+</sup> waves and subsequent activation of NCX. An up-regulation of NCX was also reported and this, coupled with the spontaneous release, led to membrane depolarization producing delayed afterdepolarizations.<sup>5</sup> This agrees with the observation of an earlier study showing an increased

\* Corresponding author. Tel: +32 16 330815, E-mail: Karin.Sipido@med.kuleuven.be (K.R.S.); Niall.Macquaide@glasgow.ac.uk (N.M.)

© The Author 2015. Published by Oxford University Press on behalf of the European Society of Cardiology.

This is an Open Access article distributed under the terms of the Creative Commons Attribution Non-Commercial License (<http://creativecommons.org/licenses/by-nc/4.0/>), which permits non-commercial re-use, distribution, and reproduction in any medium, provided the original work is properly cited. For commercial re-use, please contact [journals.permissions@oup.com](mailto:journals.permissions@oup.com)

frequency of spontaneous  $\text{Ca}^{2+}$  waves and sparks in patients with AF.<sup>6</sup> While changes in RyR phosphorylation have been emphasized, reduced expression has also been reported.<sup>7</sup> However, there is no data on a possible change in the organization of RyR. Data from animal models similarly highlight a role for altered RyR function in AF, though studies in permanent and persistent AF are limited. In the dog with heart failure and with AF, abnormal  $\text{Ca}^{2+}$  release has been reported as well as increased RyR phosphorylation.<sup>8</sup> In sheep with persistent AF, T-tubule re-organization was evident, but we also found that RyR expression was reduced, although confocal immunofluorescence imaging revealed no change in RyR distribution and density.<sup>9</sup> This hints at an underlying remodelling of RyR ultrastructural organization.

RyR clusters have previously been studied using electron microscopy of freeze fracture in thin slice preparations of skeletal and cardiac tissue. From these measurements, RyR clusters were shown as contiguous crystalline arrays of single RyR molecules. Recently developed methods allow the measurement of intracellular structures based on immunostaining in myocytes, below the traditional fluorescence resolution limits, the so-called super-resolution microscopy, including STED (STimulated Emission Depletion) and dSTORM (direct Stochastic Optical Reconstruction Microscopy).<sup>10–12</sup> Study of RyR clusters in ventricular cardiac myocytes has shown that RyR clusters have a higher, though fragmented organization, with small and large clusters grouped together in formations termed 'superclusters'.<sup>13,14</sup> These may act together to release  $\text{Ca}^{2+}$ , observed as a  $\text{Ca}^{2+}$  spark, and such grouping of RyRs is also referred to as a  $\text{Ca}^{2+}$  release unit (CRU).<sup>13,15,16</sup> In the case of atrial cells as studied here, these are frequently not coupled with the sarcolemma.<sup>9,17</sup> Modelling has revealed that RyR cluster behaviour may relate to their size; small clusters are proposed to have lower levels of allosteric regulation via coupled gating and so fire more readily, contributing more to diastolic release.<sup>16,18</sup> Similarly, preferential inhibition of small RyR clusters has highlighted their involvement in the initiation of spontaneous  $\text{Ca}^{2+}$  waves.<sup>19</sup> In this study, it was hypothesized that small clusters would act to relay  $\text{Ca}^{2+}$  release to neighbouring clusters and that this was particularly important in gaining critical mass for the initiation of a  $\text{Ca}^{2+}$  wave. It is conceivable that abnormal fragmentation of RyR clusters within CRUs may assist in the process of inter-cluster activation which initiates  $\text{Ca}^{2+}$  waves, but so far this has not been studied.

In the present study, we have investigated RyR cluster morphology in an established sheep model of persistent AF.<sup>9,20</sup> To this end, we carried out super-resolution measurements of RyR, to explore cluster size, shape, and fragmentation using STED microscopy. We defined functional CRUs as a group of clusters within 150 nm distance of each other, allowing cluster–cluster interaction.<sup>13,15</sup> In the same cells, we measured subcellular  $\text{Ca}^{2+}$  release to assess the functional changes that occur in AF. We use computational modelling to predict the impact of the altered organization of RyR clusters and CRUs on  $\text{Ca}^{2+}$  release, comparing predictions to observations of spark properties. We demonstrate that CRU morphology is a crucial determinant of the diastolic  $\text{Ca}^{2+}$  release process, which may further potentiate aberrant  $\text{Ca}^{2+}$  release in persistent AF.

## 2. Methods

A detailed description is available in the Supplementary material online.

The sheep model and atrial myocyte isolation were as described before.<sup>9</sup>

For STED microscopy, myocytes were fixed immediately after isolation in 2% paraformaldehyde.

Fixed myocytes were labelled with a primary RyR2 antibody and Alexa 647N secondary. Samples were imaged on a custom-built STED microscope<sup>21</sup> (see Supplementary material online, *Figure S1*) and analysed using custom software written in Python.

$\text{Ca}^{2+}$  sparks were measured in permeabilized myocytes perfused with a mock intracellular solution containing Fluo-3 (20  $\mu\text{mol/L}$ ) with a free  $\text{Ca}^{2+}$  of 150 nmol/L.  $\text{Ca}^{2+}$  sparks were analysed using custom software based on the Cheng algorithm.<sup>22</sup>

Computer modelling of  $\text{Ca}^{2+}$  release was based on a modified version of a previous model<sup>23</sup> using an Ultrafast Monte Carlo method, with the inclusion of localized RyR  $\text{Ca}^{2+}$ -sensing domain.

Data are presented as mean  $\pm$  SEM for RyR clusters and otherwise as scatter plots for individual cells. To include both  $N$  animals and  $n$  cells in the analysis, a hierarchical method was used.

## 3. Results

### 3.1 Near single RyR resolution by STED microscopy

Images of sub-resolution (20 nm) crimson beads were collected. The average of three aligned beads was calculated, and the profile was fitted with a Gaussian function to assess lateral resolution (*Figure 1A*). Given RyR size (30 nm), this translates to a potential resolution of 1–2 individual RyR tetramers. *Figure 1B* shows a typical myocyte imaged using confocal microscopy. *Figure 1C–F* shows the image of a 3-sarcomere-wide region, with RyRs visible along the Z-lines. Improvements in resolution are evident from conventional confocal (*C*) to the STED (*D*) and then deconvolved STED images (*E*). After deconvolution, automated thresholding was possible (*F*). *Figure 1G* shows a typical image of 10 clusters of contiguous RyRs resolved by this method, illustrating the highly variable size and shape. Cluster images were used as a mask, and the approximate RyR number that could fit into each cluster was calculated using a grid of RyR sized units (30  $\times$  30 nm) (*Figure 1H*). Given the limits of resolution, this method had limited utility if clusters had less than two RyRs; therefore, the number of RyRs per cluster will be stated as approximate.

### 3.2 RyR cluster size is unaltered in Ctrl and AF

There were no immediately apparent differences in RyR clusters of Ctrl and AF myocytes (*Figure 2A* and *B*). To ascertain whether RyR clusters were different in AF, pertinent metrics of morphology were developed and examined in 14 myocytes from 4 animals in each group. Mean cluster size was similar,  $15.4 \pm 0.4$  RyRs per cluster vs.  $15.3 \pm 0.6$  ( $n_{\text{clusters}} = 2581$  and 1261 in Ctrl and AF, respectively, *Figure 2C*). The distribution of RyRs as a function of cluster size is shown in *Figure 2D*. The relationship is well fit with the sum of an exponential for small clusters and a Gaussian function for larger clusters ( $R^2 = 0.60$  in Ctrl and 0.59 in AF). This indicates that small and large RyR clusters belong to two sub-populations. The Gaussian peak at  $\sim 50$  RyR indicates that of the larger population, this is the most common cluster size in both AF and Ctrl. The cumulative histogram of RyR cluster size (*Figure 2E*) shows that most RyRs reside in small clusters, with over half of all RyR residing in clusters containing six RyRs or less. Assessment of the proximity between individual RyR clusters (*Figure 2F*) shows that clusters are closer together in AF. Mean centroid distance was reduced by 23% in AF.

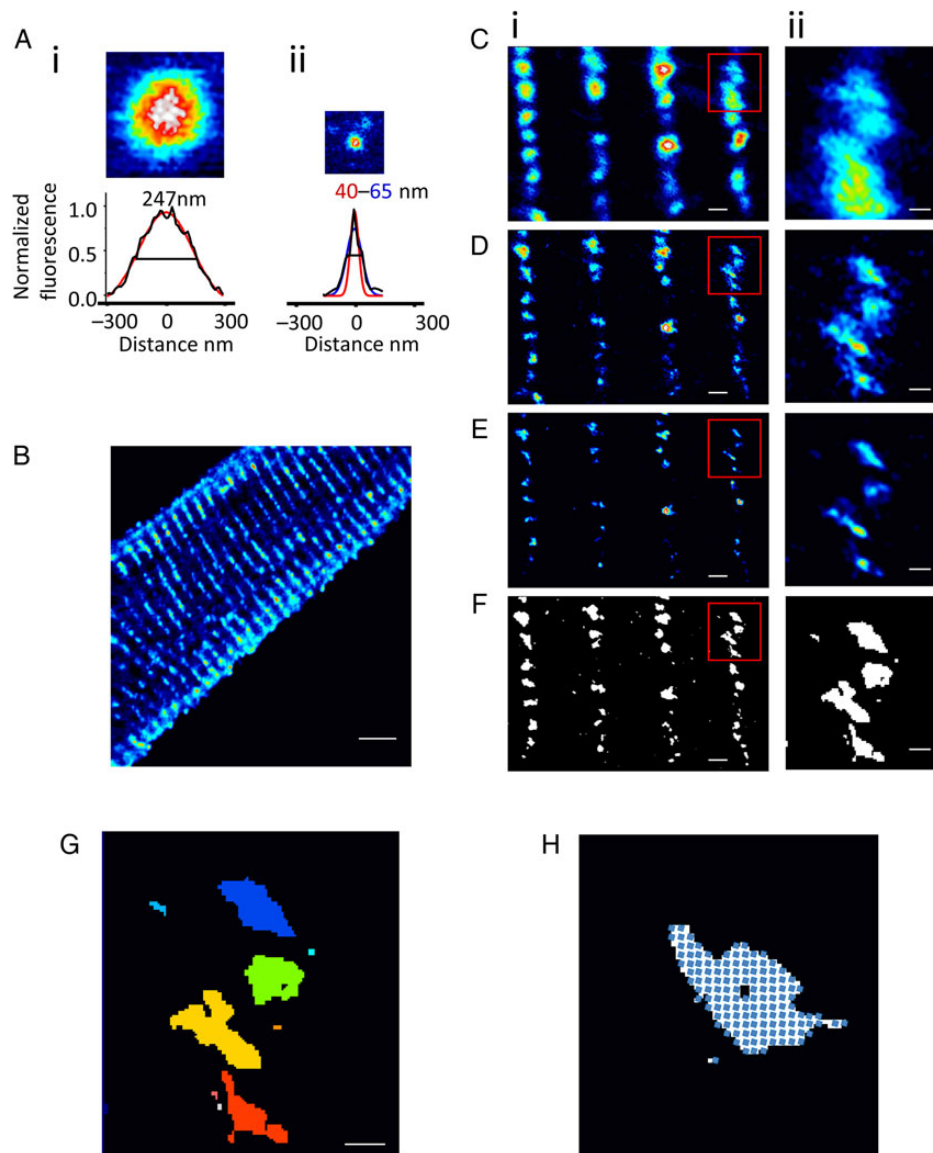


**Figure 1** Deconvolved STED microscopy resolves RyR sub-cluster formations in atrial myocytes. (A) Average of the same three fluorescent beads aligned on their peaks from confocal (i) and STED (ii) recordings, allowing a  $\sim 4\text{--}6\times$  improvement in resolution. (B) RyR antibody labelling in an atrial myocyte visualized using confocal microscopy. (C–F) Optical and software-based methods used to allow RyR cluster resolution in a region of an atrial myocyte (i), with further zoom in of the region outlined in red (ii). (C) Conventional confocal image; (D) the raw STED image; (E) after deconvolution noise is reduced with more defined edges of each sub-cluster; (F) RyR clusters are thresholded to allow morphology quantification. (G) Individual colours delineate 10 clusters taken from F (ii). (H) Method for RyR cluster size quantification: a grid of single RyRs (blue squares) are superimposed on the thresholded image. Scale bars: (B)  $5\ \mu\text{m}$ ; (G–F)  $250\ \text{nm}$ ; (Cii–Fii)  $100\ \text{nm}$ .

### 3.3 Organization of CRUs is different in AF

Experimental work has shown RyRs within clusters interact via coupled gating.<sup>24</sup> Theoretical work has shown this would mean that small clusters behave differently<sup>18</sup> and may have a role in the generation of  $\text{Ca}^{2+}$  waves.<sup>19,25</sup> It has been speculated that clusters that are close together will also interact to trigger release if they are within  $100\ \text{nm}$  of each other, forming functional release units.<sup>13</sup> Our modelling (below) indicated that a distance of  $\leq 150\ \text{nm}$  yields a high probability of cluster–cluster interaction; therefore, RyR clusters were grouped when edge-to-edge distances were  $\leq 150\ \text{nm}$  (Figure 3A). This enables additional quantification of CRU organization, relevant to their function.

Using these grouping criteria, Figure 3B–D shows that CRUs are larger in AF with more clusters in a CRU and a higher total number of RyRs.

To assess the internal organization within a CRU, the ratio of cluster filled with RyR to the total CRU area was calculated (Figure 3E). CRU's in AF were less filled with RyR indicating a higher degree of fragmentation in AF.

### 3.4 A high proportion of RyR clusters are not along the Z-line in AF

The initiation of  $\text{Ca}^{2+}$  waves is highly sensitive to longitudinal sarcomeric CRU separation which may be reduced in hypertrophy.<sup>26</sup> No

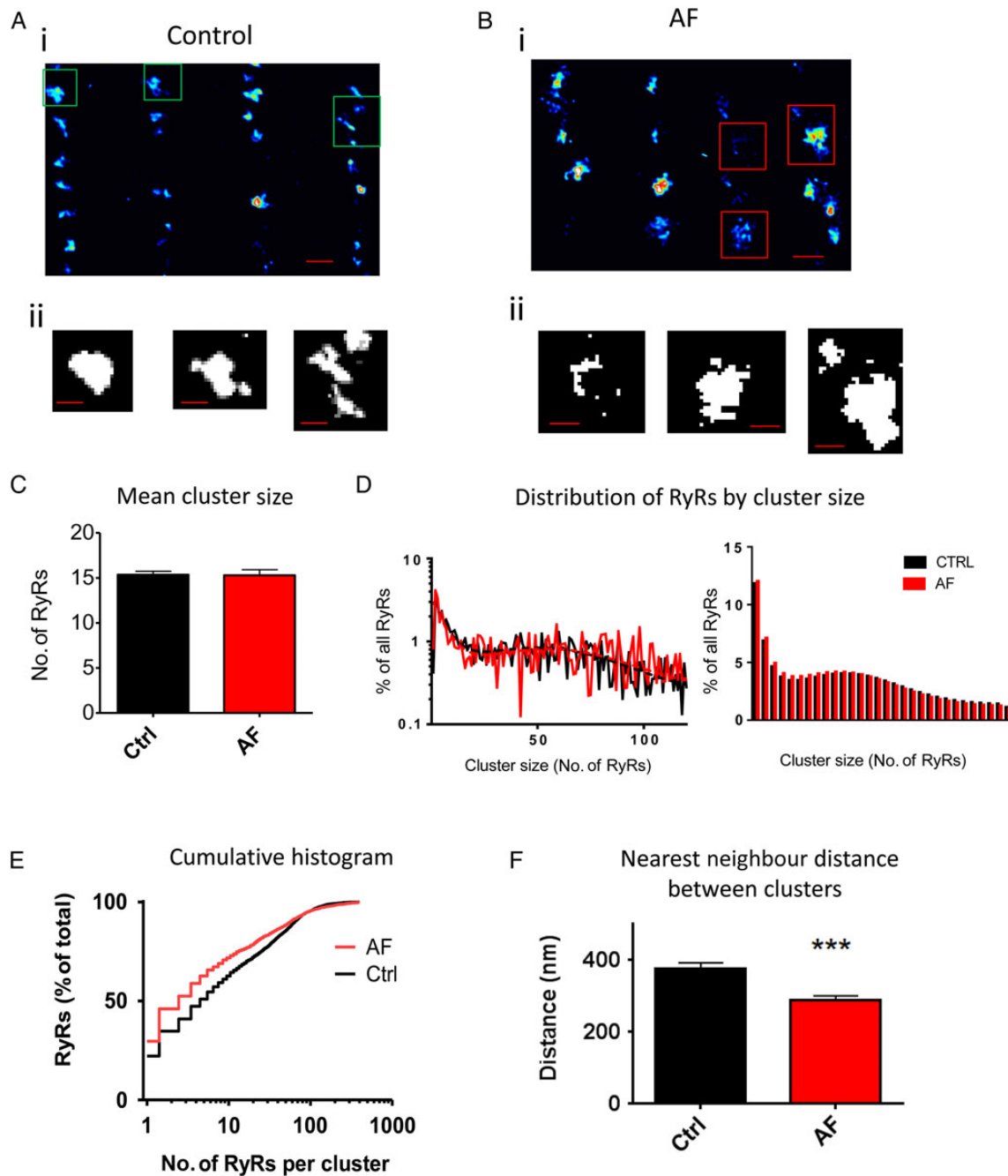


**Figure 2** Quantification of RyR cluster size. (A and B) Typical deconvolved STED (i) and thresholded STED (ii) from Ctrl and AF cells; scale bars: upper panel 500 nm, lower 200 nm. (C) Mean RyR cluster size;  $n_{\text{clusters}} = 2581$  and  $1261$ ,  $n_{\text{cells}} = 14$  and  $14$  in 4 Ctrl and 4 AF animals, respectively. (D) Distribution histogram of RyRs (fraction of the total number of RyRs) as a function of RyR cluster size in Ctrl (black) and AF (red). The two distributions have been fit with the sum of an exponential and Gaussian distribution; right panel with bin size 10. (E) Cumulative histogram of the distribution of RyRs according to cluster size (same data as in D). The majority of RyRs reside in clusters containing  $<6$  RyR. (F) Mean nearest neighbour distance between individual RyR clusters in Ctrl and AF, quantified by distances between the centre of each cluster ( $***P = 0.006$ ). Data are mean  $\pm$  SEM.

such alteration in sarcomere length was observed here, but the presence of RyR clusters between Z-lines could facilitate propagation. To investigate this, the minimum separation of large ( $>10$  RyR) clusters in the longitudinal axis was quantified (Figure 3F). Small clusters ( $<6$  RyR) were excluded on the basis that their  $\text{Ca}^{2+}$  release would only allow propagation over a short distance (100–150 nm). A histogram of minimum RyR cluster separation in the longitudinal axis (Figure 3G)

shows that many more clusters are  $<1 \mu\text{m}$  apart in AF; the median of the histogram is 920 nm in AF vs. 1300 nm in Ctrl. Similarly, in AF a larger proportion ( $11.0 \pm 0.1$  vs.  $5.7 \pm 0.9\%$  in Ctrl) of RyR clusters were found between Z-lines (see Supplementary material online, Figure S2). This shows that dispersion of RyR clusters away from the Z-line is more pronounced in AF, narrowing the distance  $\text{Ca}^{2+}$  needs to diffuse across the sarcomere to activate neighbouring CRUs.

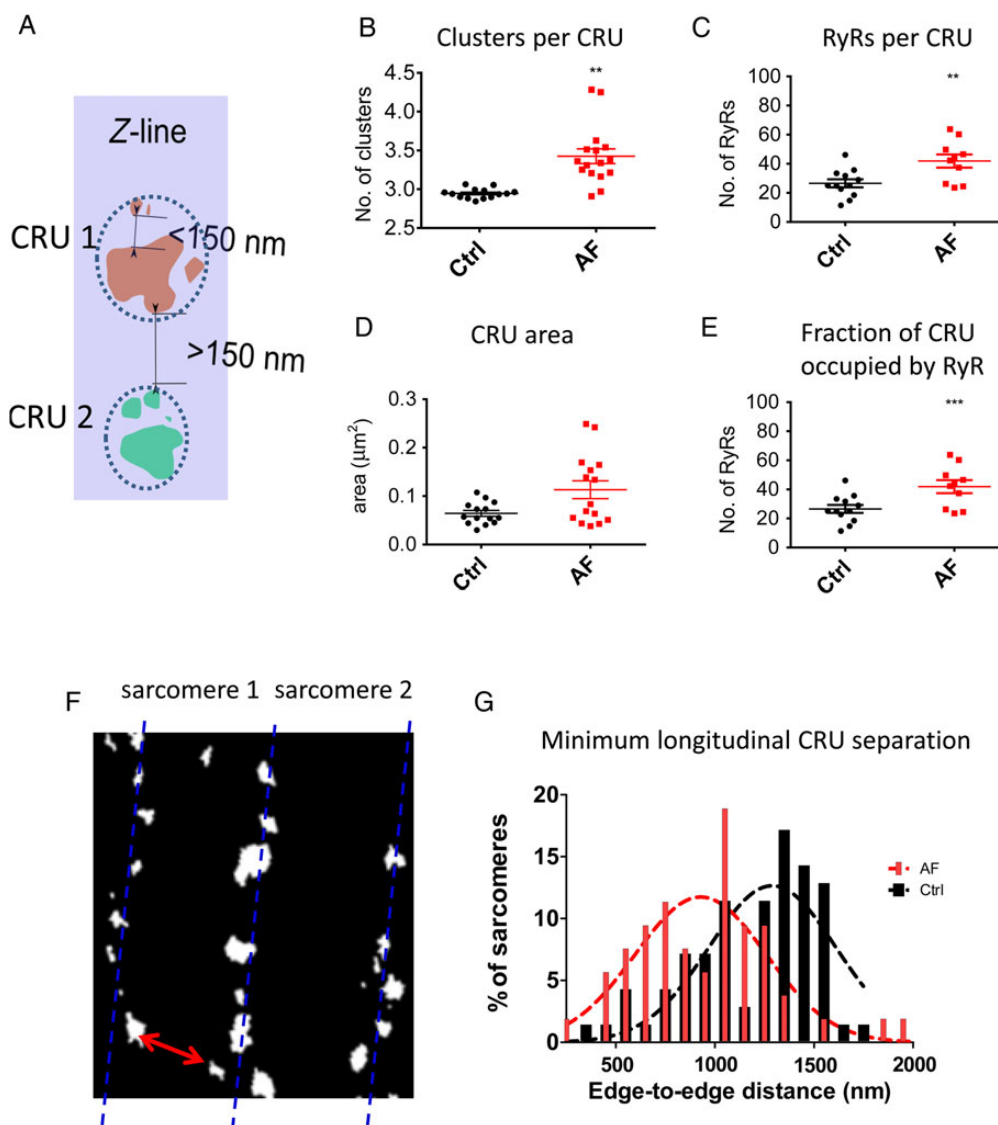


**Figure 3** Quantification of alterations of CRU morphology and separation in AF. (A) Criteria for cluster grouping within CRUs defined as functionally grouped clusters if within the 150 nm edge to edge of each other (shown all of similar colour). (B) Mean number of clusters per CRU ( $n$  cells and sheep as in Figure 2,  $**P = 0.015$ ). (C) Number of individual RyRs per CRU ( $**P = 0.0015$ ). (D) The area occupied by a CRU within minimal bounding polygon (see Supplementary material online,  $P = 0.14$ ). (E) The fraction of CRU occupied by RyR was quantified as a ratio of RyR: total area per CRU, which is inversely related to the degree of CRU fragmentation ( $***P = 0.0001$ ). (F) Quantification of the minimum separation of RyRs in the longitudinal direction (red arrow as an example of measured distances). (G) Histogram of the minimum separation in the longitudinal direction showing that in AF more sarcomeres have CRUs that are closer together in the longitudinal direction.

### 3.5 Functional alterations in spark frequency and kinetics in AF

To assess RyR cluster function, freshly isolated cells were permeabilized and perfused with a mock intracellular solution to enable the observation of spontaneous sparks (Figure 4A).

Most notably, macrosparks and double release sparks were observed in AF, but not in Ctrl (Figure 4B). Single  $\text{Ca}^{2+}$  spark properties were also different (Figure 4C). Frequency was markedly higher in AF (Ci) and width was lower (Cii), implying a smaller  $\text{Ca}^{2+}$  flux per release event on average. Differences in spark kinetics were also evident; duration (Ciii) and time to peak (Civ) were prolonged in AF, by 15 and 18%, respectively, and illustrated by example (Figure 4D). However, SR

content in permeabilized myocytes was not different (see Supplementary material online, Figure S3).

### 3.6 Co-activation of RyR clusters within a functional CRU

A stochastic model of RyR was used to assess how the organization of RyRs affects the function of individual clusters and their interaction within functional CRUs. Here a temporal and spatial model of  $\text{Ca}^{2+}$  sparks with single channel kinetics was used, based on a previous model,<sup>27</sup> adapted to the permeabilized atrial myocyte (see Supplementary material online). In a first simulation, the probability of one small cluster (5 RyRs) being triggered by the opening of a larger neighbouring

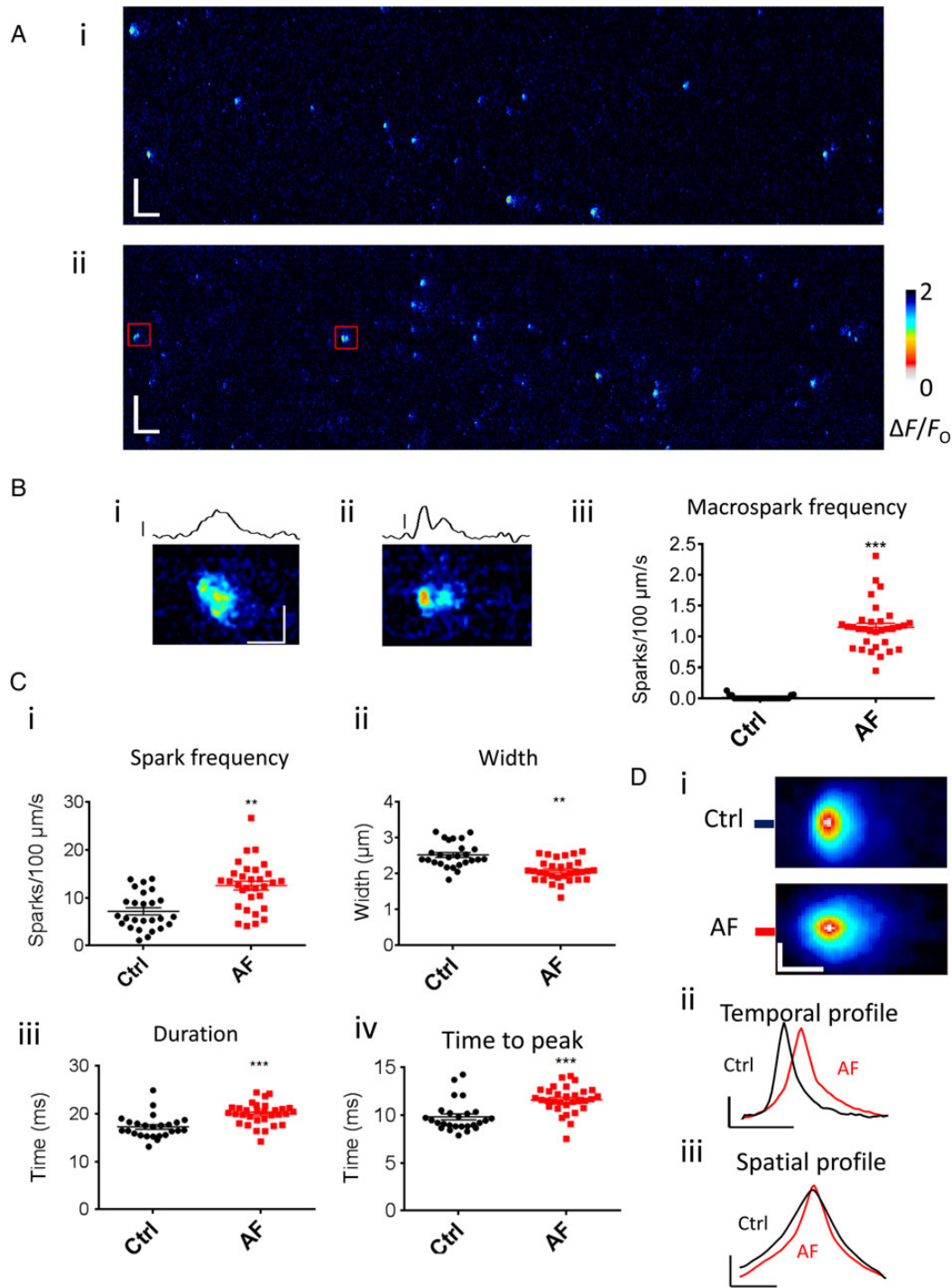


**Figure 4** More frequent  $\text{Ca}^{2+}$  sparks, with slowed kinetics in permeabilized AF myocytes. (A) Examples of line scan images of spark recording in Ctrl (i) and AF (ii); rectangles highlight macrosparks. (B) Examples of two types of macrosparks in AF: multisite (i, from left box in Aii) and single site (ii, from the right box in Aii); macrospark incidence was increased in AF (iii). (C) Mean spark parameters show increase in spark frequency (i, \*\*\*\* $P = 0.045$ ), a reduced width (ii, \*\*\* $P = 0.001$ ), a longer spark duration (iii, \*\*\* $P = 0.0001$ ), and time to peak (TTP, iv, \*\*\* $P = 0.004$ ) in AF.  $N_{\text{cells}} = 26$  and 31 in 5 Ctrl and 6 AF animals, respectively. (Di) Average linescans of all sparks in a typical Ctrl and AF cell ( $N = 179$  and 258) with their temporal and spatial profiles from the central three pixels (lines on left indicate regions taken). Scale bar = 10  $\mu\text{m}$  and 100 ms in (A); 5  $\mu\text{m}$  and 50 ms in (B); 20 ms and 2  $\mu\text{m}$  in (Di), 0.2  $\Delta F/F_0$  and 20 ms in (Dii); 0.2  $\Delta F/F_0$  and 2  $\mu\text{m}$  in (Diii).

cluster (49 RyRs) was assessed (Figure 5A). A pseudo-linescan image of the total  $\text{Ca}^{2+}$  (Figure 5Bi) highlights a mild asymmetry on the lower side of the image due to the activation of the small cluster. This is

indiscernible on the resulting  $F/F_0$  image (Figure 5Bii), but is visible in spatial profiles of total  $\text{Ca}^{2+}$  (Figure 5Ci) and fluorescence (Figure 5Cii) at the time points indicated. Given this occurs after the

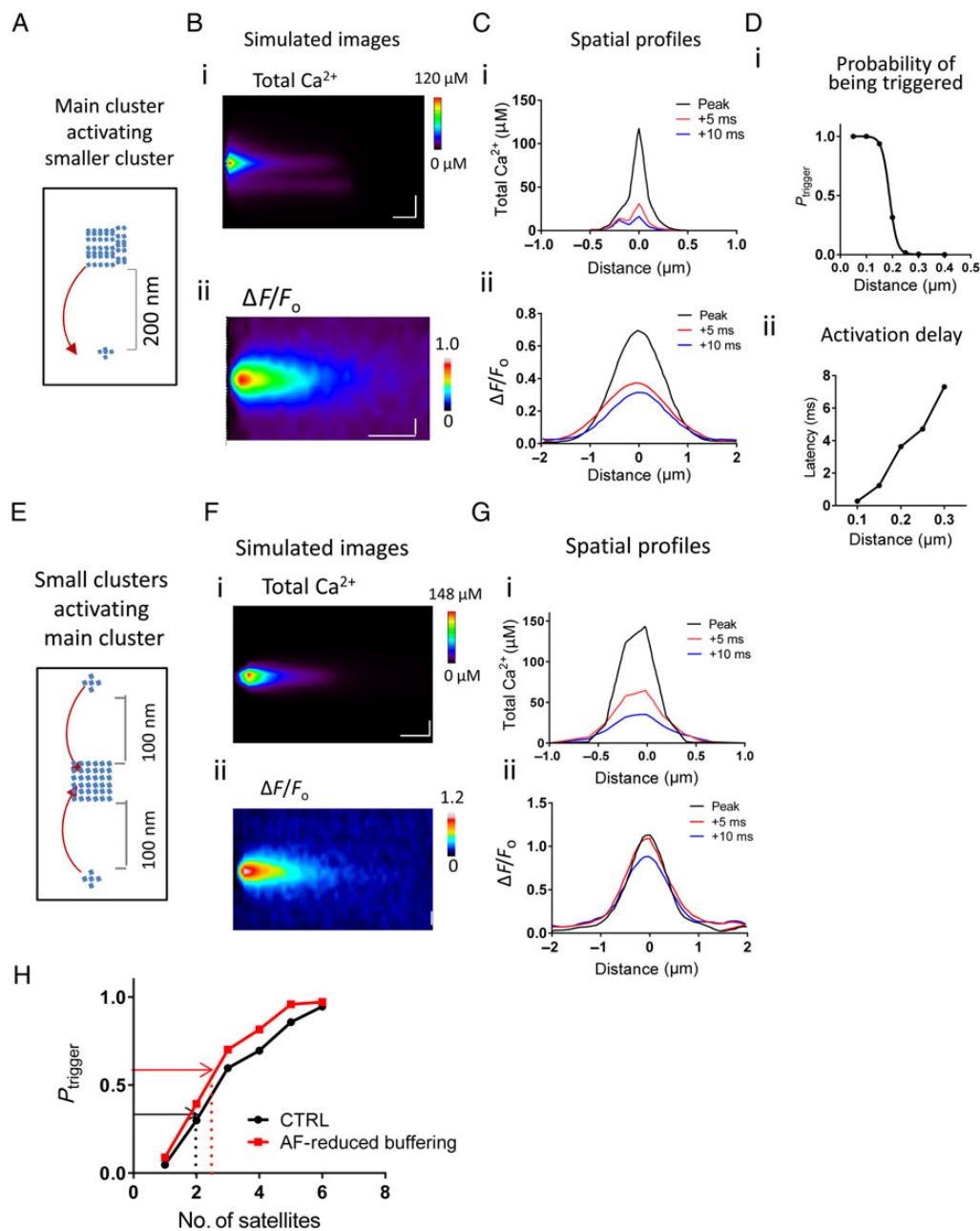


**Figure 5** Computational modelling of intra-CRU RyR interaction. (A) Schematic of model for simulation: release from one large RyR cluster within the CRU can activate the smaller RyR cluster by the diffusion of released  $\text{Ca}^{2+}$  from the larger cluster (depicted by the red arrows); the 49 RyR large cluster is 200 nm edge to edge away from the 5 RyR cluster. (B) Simulated linecan image of total  $\text{Ca}^{2+}$  (i): A smaller, more prolonged release from the small cluster is visible, after activation by  $\text{Ca}^{2+}$  released from the main cluster; however, this is not visible on the simulated linecan  $F/F_0$  image (ii). (C) Spatial profiles of total  $\text{Ca}^{2+}$  (i) and  $F/F_0$  (ii) at different time points after peak release (inset). Cluster interaction is only evident as asymmetry in the total  $\text{Ca}^{2+}$  plot at  $-0.1$  and  $-0.2$  distances. (D) Probability of release from a small cluster being triggered ( $P_{\text{trigger}}$ ) as function of the distance from the larger site (i) and the corresponding delay of activation (ii). There is a high likelihood of activation with  $<2$  ms delay if small clusters are  $\leq 150$  nm away from a larger one. (E) Schematic of model for simulation: synchronous release from small (5 RyR) clusters can activate a larger (25 RyR) cluster 100 nm away by the diffusion of released  $\text{Ca}^{2+}$  (red arrows). (F) Simulated linecan images of total  $\text{Ca}^{2+}$  (i) and resultant  $F/F_0$  (ii). (G) Spatial profiles of total  $\text{Ca}^{2+}$  (i) and  $F/F_0$  (ii) at times indicated after the peak of release. (H) Simulated probability of triggering a central cluster with increasing numbers of satellite RyR clusters. Dotted lines indicate experimentally observed numbers of satellites in Ctrl (black) and AF (red). Scale bars: (Bi and Fi): 200 nm, 5 ms; (Bii and Fii): 500 nm, 20 ms.

peak of the main release, it would be undetectable by traditional spark analysis. The key finding from this simulation was the relationship describing the probability of small clusters being triggered ( $P_{\text{trigger}}$ ) as a

function of their distance from the main cluster (Figure 5Di). The relatively steep drop at  $\sim 150$  nm from 0.937 to 0.315 indicates that small clusters  $\geq 150$  nm away are unlikely to be influenced by release from

the main cluster. This demarcates an effective 150 nm sphere of influence of this mode of activation. The delay in activation of the small clusters (Figure 5Dii) was negligible ( $<2$  ms) for distances  $\leq 150$  nm.

### 3.7 Spark probability is increased in more fragmented CRUs

The probability of small clusters within a CRU to trigger larger neighbouring clusters ( $P_{\text{trigger}}$ ) was further investigated. A varying number of small (5 RyR) clusters were set to open simultaneously, the  $\text{Ca}^{2+}$  released then diffused to the larger cluster (25 RyR), triggering activation (Figure 5E). Simulated pseudo-linescans of total  $\text{Ca}^{2+}$  and  $\Delta F/F_0$  from a two satellite-triggered release show a higher amplitude, longer duration release (Figure 5F) even more visible on the temporal profiles (Figure 5G), with  $F/F_0$  values remaining high 5 ms after the peak release, in contrast to the more rapid fall shown in Cii (compare traces at 10 ms).

In AF, cells showed increased fragmentation of CRUs. To explore the functional implications of this, the number of satellite clusters around a large cluster was increased. The probability of triggering release from the larger cluster by these satellite clusters had a very steep dependence on the number of satellite clusters (Figure 5H). In AF, the number of satellites increased from 2 to 2.5 (3 to 3.5 clusters per CRU); combined with the reduced buffering found in AF (see Supplementary material online, Figure S3), this increased the likelihood of release triggered in this way by  $\sim 75\%$  (dotted lines in Figure 5H), approximating the increase in spark frequency observed experimentally.

Modelling shows the spark frequency of small clusters to be comparatively higher (see Supplementary material online, Figure S5), thereby increasing the likelihood of all satellites synchronizing, activating release. Nevertheless, the 75% increase may represent more of an upper limit as satellites may be  $>100$  nm away. Even given these caveats, higher CRU fragmentation and reduced buffering would both facilitate intra-cluster interaction, leading to an increased spontaneous spark rate.

### 3.8 Modelling sarcomeric $\text{Ca}^{2+}$ propagation

One notable difference in AF was the appearance of release events propagating across sarcomeres, macrosparks. Shorter sarcomere lengths can greatly increase the probability of this type of propagating release,<sup>11</sup> but this was not observed here. However, higher incidence of clusters between Z-lines (see Supplementary material online, Figure S4) and shorter distance between clusters in the longitudinal axis (Figure 3F) may have similar effects.

To investigate this, we simulated four clusters with varying separation (Figure 6A, 400–700 nm). These clusters with 25 RyRs each had three small (5 RyR) clusters 100 nm apart, simulating CRU geometry in AF. With this configuration, the probability of propagation between the clusters was 100% when 400 nm apart, (Figure 6D). This fell rapidly as clusters were moved further than 500 nm apart but allowed for formation of macrosparks, as simulated in Figure 6B and C where four clusters were placed 600 nm apart. Triggering the two central clusters allowed propagation (with a  $\sim 6\%$  chance). The  $F/F_0$  image of this event had a FWHM of  $\sim 5$   $\mu\text{m}$ , similar to that observed experimentally. This simulation highlights how RyR cluster dispersion could lead to the genesis of macrosparks by providing a relay system to allow propagation across sarcomeres.

## 4. Discussion

Using STED microscopy, RyR cluster morphology in atrial myocytes could be analysed in detail, revealing fragmentation of CRUs in

persistent AF. This nanoscale remodelling impacts on unitary  $\text{Ca}^{2+}$  signalling, as shown experimentally and through simulation.

### 4.1 RyR cluster organization in atrial cells and remodelling with AF

STED microscopy allowed us to visualize immunostained RyR clusters at a resolution of around 60 nm; deconvolution allowed further improvements in image resolution and quality. Similar methods have recently been used to resolve T-tubule structures in living ventricular myocytes.<sup>28</sup> This compares somewhat less favourably to the resolution of 20–30 nm obtained using STORM.<sup>12</sup> STED offers the advantage of allowing access to the centre of the cell, with reduced acquisition time, and is less prone to artefacts of densely stained samples; however, the experimental setup is more complex.

In their pioneering work using STORM imaging, Baddeley et al.<sup>13</sup> reported on RyR organization in peripheral clusters close to the membrane surface. The assumption was that sampling of peripheral clusters implied a more flat geometry, therefore facilitating measurement of complete clusters. As we are sampling more at the centre, this assumption cannot be made. Given the axial resolution of STED, we can assume we are actually sampling from a layer of  $\sim 0.5$   $\mu\text{m}$ . Despite these differences in technique, in depth within the cell, in species and cardiac region, there is a remarkable similarity in the ultrastructural properties of cluster size and organization between the two studies. Likewise we find that on average there are  $\sim 15$  RyRs per cluster, but with a broad distribution of cluster sizes. This similarity between studies is surprising, but may highlight a common mechanism governing the process of cluster formation. Further analysis in the current study suggests two sub-populations of RyR clusters. The most numerous consists of small clusters containing six or less RyRs; the second has a broader distribution with predominance at  $\sim 50$  RyR clusters. This value is slightly higher than a recent 3-D analysis of  $\text{Ca}^{2+}$  sparks in cat atrial myocytes, which calculated the flux produced from typical sparks originated from 20–30 RyRs,<sup>29</sup> but lower than the  $\sim 80$  RyRs estimated from deconvolved confocal images<sup>30</sup> or  $\sim 63$  RyRs using dSTORM<sup>14</sup> in rat ventricular myocytes. This disparity between the studies may be due to incomplete activation of all RyR clusters per CRU during each spark event. However, species differences in CRU morphology cannot be discounted.

Remarkably, the primary assembly of RyR clusters appears to be unaltered in AF, as cluster size was unchanged. However, the organization of the individual clusters into functional CRUs is different. In AF, there are more RyRs per CRU, yet within CRUs these clusters are less densely packed, resulting in a larger CRU area with a more fragmented CRU morphology. Of note, total RyR protein expression levels are slightly lower<sup>9</sup> (see Supplementary material online, Figure S6), which could contribute to more dispersed clusters. It is tempting to speculate that changes in CRU morphology may relate to the fragmentation of the T- and axial tubular (TAT) structure in AF<sup>9</sup> or atria from heart failure.<sup>17</sup> Proteins associated with RyR such as junctophilin-2 (JPH2) and more recently BIN-1<sup>31</sup> have been implicated in the TAT organization,<sup>32,33</sup> and it is conceivable that these play a role in the secondary RyR organization. Low levels of JPH2 have been implicated in AF.<sup>34</sup> Alternatively, alterations in SR geometry may occur in AF and affect RyR cluster formation. SR geometry changes have been reported in ventricular myocytes from mice with genetically altered SR proteins.<sup>35,36</sup> This could also have implications for sparks properties by altering SR  $\text{Ca}^{2+}$  depletion rates.<sup>37</sup> Further study is required to assess these processes.



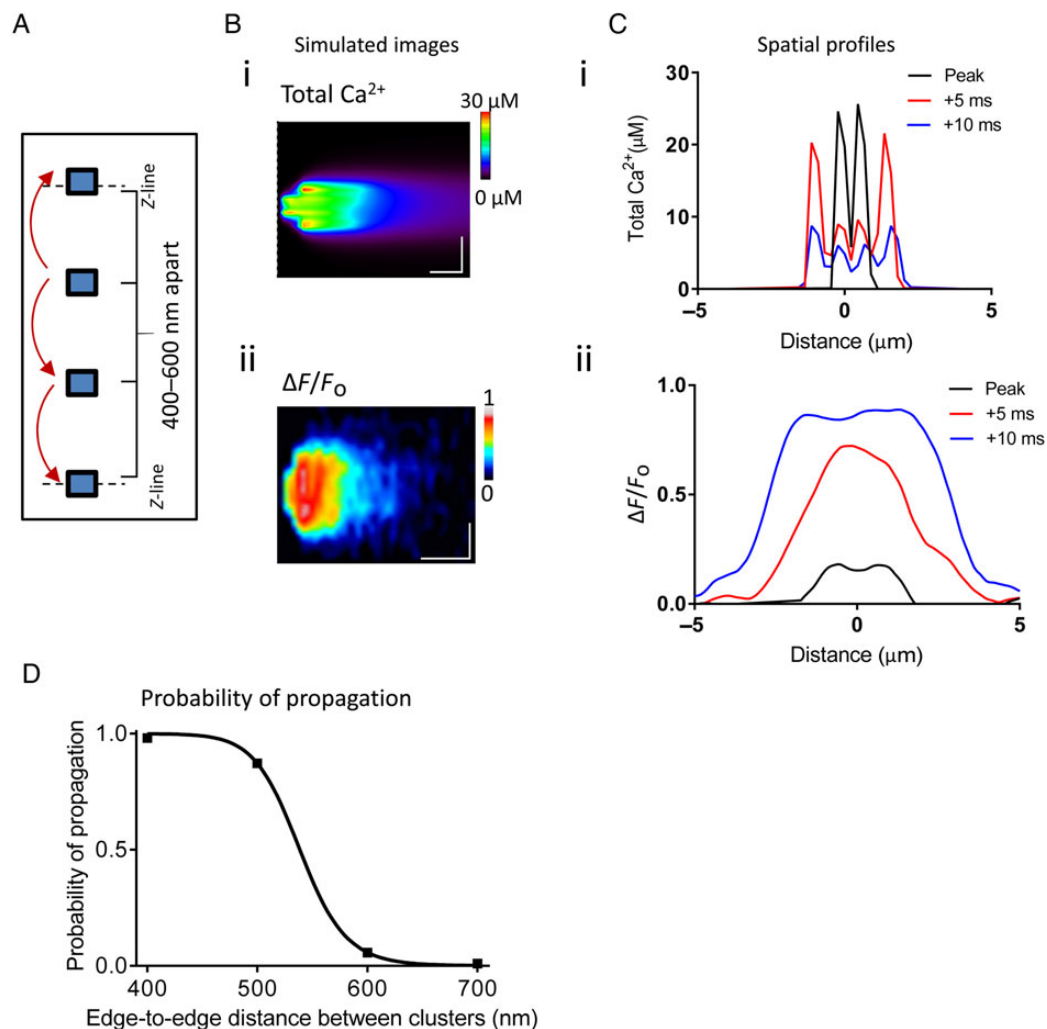


**Figure 6** Simulation of neighbouring cluster activation during a macrospark. (A) Schematic of the model: four clusters, each with one central 25 RyR cluster and three clusters with 5 RyR, placed at variable edge-to-edge distances, from 400 to 700 nm. (B) Simulated linescan image of a macrospark event. Four clusters were placed 600 nm apart; the central release site from one was activated, releasing  $\text{Ca}^{2+}$  that diffused to raise  $\text{Ca}^{2+}$  local to the neighbouring site, triggering its release. Resultant total  $\text{Ca}^{2+}$  (i) and  $F/F_0$  linescan images (ii) from this simulation are shown. (C) Spatial profiles of the  $\Delta F/F_0$  and total  $\text{Ca}^{2+}$  are depicted at the timescales indicated. (D) Probability of propagation between adjacent clusters, analogous to the probability of macrospark formation, as a function of the longitudinal separation between them. Scale bars in B: 2  $\mu\text{m}$  vertical (i and ii), 5 ms (i) and 20 ms (ii) horizontal.

## 4.2 Cluster re-organization leads to increased RyR release activity

In the current study, functional properties of RyR were measured in permeabilized cells at 150 nmol/L  $\text{Ca}^{2+}$ . The permeabilized cell preparation allows a high degree of control over the intracellular environment without confounding factors of surface membrane transport, sub-membrane  $\text{Ca}^{2+}$  microdomains, or CaMKII activation.<sup>38</sup> It is particularly suited to study the properties of RyR clusters during direct activation by the prevailing  $\text{Ca}^{2+}$  while preserving cluster structure and interaction, as opposed to bilayer experiments. Our findings in AF myocytes of an elevated spark frequency and high occurrence of locally propagating  $\text{Ca}^{2+}$  release events (macrosparks) therefore can be most likely attributed to the changes in RyR cluster organization. Computational modelling supports this hypothesis.

A major element appears to be the close proximity of multiple small clusters within a CRU which could drastically increase the probability

of a CRU to fire. Indeed, our modelling suggests that over half of all sparks may be due to triggering by smaller clusters. RyR cluster size has been predicted to affect release; coupled gating and allosteric interaction via FKBP12.6 may regulate the probability of RyR cluster opening.<sup>24</sup> A configuration with more small clusters per CRU may underlie repetitive or hyperactive spark sites.<sup>39–41</sup> However, recent evidence has emphasized that local  $\text{Ca}^{2+}$  release causing CICR from neighbours within each cluster is the prime determinant of RyR behaviour, influencing  $\text{Ca}^{2+}$  spark frequency and release duration.<sup>42</sup> Thus, although the mode of interaction is presently under debate, the consensus is that RyRs in close proximity interact and influence CRU behaviour.

Previous modelling and experimental data have suggested that small RyR clusters could underlie non-spark-mediated loss of  $\text{Ca}^{2+}$  in the regulation of SR content<sup>18,43</sup> and participate in the initiation of spontaneous  $\text{Ca}^{2+}$  waves.<sup>19</sup> The current modelling and experimental data indicate that the presence of more small RyR clusters within CRUs also

contributes to  $\text{Ca}^{2+}$  sparks, leading to a higher  $\text{Ca}^{2+}$  spark rate in AF compared with Ctrl. Primarily this is due to smaller clusters within the functional group opening ( $>20\times$ ) more often than larger clusters. When these cluster openings synchronize, they can trigger release from clusters close by. In AF, this fragmented CRU geometry is more prevalent, given that the mean number of clusters per CRU increases from 3 to  $\sim 3.5$ .

Sarcomeres with clusters bridging the sarcomeric separation and in close proximity of each other were more common in AF. Using a simplified model for cross-sarcomere propagation, this predicted a high probability of propagation. Bridging of the sarcomere through clusters away from the Z-line could thus explain the higher macrospark frequency observed. For a macrospark, recruitment of  $>2$  clusters  $<700$  nm apart would be required. Since minimum edge-to-edge sarcomeric distances were around this order in AF, this form of secondary recruitment would have a high likelihood. Prolonged or slow sparks have been described recently in a murine model of heart failure and were hypothesized to occur due to more subdivision in each CRU.<sup>44</sup> The current study finds more striking structural and functional measurements highlighting the relevance of CRU remodelling to cardiac disease.

### 4.3 Relevance of changes in RyR cluster structure and function to the pathology of AF

Dysregulation of  $\text{Ca}^{2+}$  release and RyR, observed as increased spark activity and  $\text{Ca}^{2+}$  waves in patients with AF,<sup>4–6</sup> are considered contributing factors in AF. Altered calcium release has been attributed to secondary modification of RyR function through CaMKII-dependent phosphorylation;<sup>45</sup> oxidation or nitrosylation, described in heart failure,<sup>46,47</sup> may also be present. The current study demonstrates that remodelling at the nanoscale level may be an additional factor. The relative importance for RyR activity and AF *in vivo* is at present difficult to gauge as there are no tools that allow a direct intervention changing cluster organization/size and evaluating the impact on AF *in vivo*, as opposed to the pharmacological tools, or genetic tools in mice, that can be applied to alter phosphorylation.

An increased spark probability due to ultrastructural changes may induce a positive feedback loop of CaMKII activation in the vicinity of increased release activity. Additional phosphorylation or oxidation processes would sensitize the fragmented clusters to prevailing  $\text{Ca}^{2+}$ . Since smaller RyR clusters are proposed to be more sensitive to phosphorylation processes,<sup>18</sup> it is likely that indeed organization at the nanoscale level and functional modifications will interact in facilitating abnormal  $\text{Ca}^{2+}$  release in AF.

Reduced cytosolic buffering in AF would facilitate free diffusion of released  $\text{Ca}^{2+}$  allowing activation of adjacent CRUs. This form of inter-CRU recruitment may play an important role in the recruitment of adjacent sites in physiological  $\text{Ca}^{2+}$  waves, which occur as part of the E–C coupling process in the atria. In persistent AF, this would infer an increase in the effective gain of the  $\text{Ca}^{2+}$  release system. This effective increase in gain and reduced cellular buffering may partially compensate for the reduced L-type current and reduced T-tubule density observed, but may have detrimental effects by inducing spontaneous  $\text{Ca}^{2+}$  waves which may generate DADs, especially when NCX activity is increased as is the case in AF.<sup>5,9</sup> Whether spontaneous depolarization plays a role in the substrate of persistent AF is a matter of debate. A study on maintenance of stretch-related AF suggested interplay between rotors and

focal discharges.<sup>48</sup> Multiple small release events that are not triggering an AP may contribute to membrane instability by a small increase in net inward NCX current.

Regarding the relative role of RyR function within the overall changes in  $\text{Ca}^{2+}$  handling in AF, further computer modelling and experimental study is needed to uncover the involvement in the arrhythmic burden and contractile dysfunction. Of note, however, a number of reports highlight the occurrence of AF in patients with primary genetic RyR dysfunction.<sup>49</sup>

### 4.4 Limitations

While the resolution of the measurements here is sufficient to study RyR CRU morphology, single RyR measurements are not possible. The CRU's measured here are from  $>2$   $\mu\text{m}$  deep within the cell and therefore are not flat. Peripheral clusters are proposed to be more flat;<sup>12</sup> however, myocyte morphology will never allow perfect alignment with the coverslip. Similarly, the axial resolution of STED microscopy, while better than highly inclined TIRF mode, is still  $\sim 0.5$   $\mu\text{m}$ . These confounding factors may limit more accurate RyR cluster quantification. Alternative approaches to gain information on cluster size which include out of focus RyR, using a method previously used for confocal measurements,<sup>30</sup> are presented and discussed in the Supplementary material online, *Figure S6*.

To study  $\text{Ca}^{2+}$  sparks in the absence of  $\text{Ca}^{2+}$  waves, a moderate level (350  $\mu\text{M}$ ) of EGTA was used. The addition of cytosolic buffers is known to affect  $\text{Ca}^{2+}$  release, and recent studies<sup>43,50</sup> suggest that this may happen with  $\geq 360$   $\mu\text{M}$  EGTA, similar to that used here. If experiments had been carried out at lower buffering levels, the observed differences in spark frequency and TTP may have been more pronounced.

Differences in RyR phosphorylation, but not in FKBP12.6 or PP1 protein expression, can be detected in tissue homogenates (see Supplementary material online, *Figure S7*). However, in permeabilized cells, modification of RyR function by CaMKII (or NOS) is assumed to be absent as the intracellular milieu is clamped at  $[\text{Ca}]$  below levels necessary for activation (see Supplementary material online) and comparable for CTRL and AF. Likewise redox conditions should be similar for both groups. However, we cannot exclude microdomains maintaining differences in redox near RyR as redox potential was not clamped as in Shirokova et al.<sup>51</sup>

Coupled gating was used in the simulations here. No clear consensus on the importance of coupled gating on RyR function has yet been reached. However, it is clear that RyR opening increases the likelihood of triggering neighbours by  $\text{Ca}^{2+}$ -induced  $\text{Ca}^{2+}$  release and that this nanoscale influence has a similar effect.<sup>52</sup> This is discussed further in the Supplementary material online.

### 4.5 Conclusions

RyR clusters are highly variable in size and can be further described in a second-order organization into functional CRUs. The current data underscore the role of RyR cluster morphology and buffering in the generation of spontaneous  $\text{Ca}^{2+}$  release.

In persistent AF, more fragmented CRUs, with more clusters that are in close proximity to each other, lead to more inter-cluster interaction, potentiated by reduced  $\text{Ca}^{2+}$  buffering. Together, this leads to an overactive  $\text{Ca}^{2+}$  release with increased chance of propagating release events.

## Supplementary material

Supplementary material is available at *Cardiovascular Research* online.

## Acknowledgements

The authors thank Godfrey Smith for careful reading of the manuscript. NVIDIA Corporation is gratefully acknowledged for providing GPUs for computation to M.S.J.

**Conflict of interest:** none declared.

## Funding

This work was supported by the Belgian Science Policy Program P6/31 (K.R.S.) and P6/27 (J.H.); European Union grant Health-F2-2009-241526 EUTrigTreat (K.R.S.); the FP7 Marie Fellowship PIEF-GA-2009-255264 (N.M.); Flemish research council (FWO) grant G060212N (K.R.S. and N.M.), G.0366.06 (J.H.), clinical researcher fellowship (R.W.), postdoctoral research fellowship (I.L.); Medtronic Belgium (R.W.); JST, PRESTO grant (J.H.); IWT scholarship (W.S.); Flemish Government longterm structural funding-Methusalem (J.H.); National Institutes of Health grant R01HL105239 and R01HL105239 (M.S.J.). Funding to pay the Open Access publication charges for this article was provided by European Union grant Health-F2-2009-241526 EUTrigTreat (K.R.S.).

## References

- Wakili R, Voigt N, Kaab S, Dobrev D, Nattel S. Recent advances in the molecular pathophysiology of atrial fibrillation. *J Clin Invest* 2011;**121**:2955–2968.
- Camm AJ, Lip GY, De CR, Savelieva I, Atar D, Hohnloser SH, Hindricks G, Kirchhof P. 2012 focused update of the ESC Guidelines for the management of atrial fibrillation. *Eur Heart J* 2012;**33**:2719–2747.
- Dobrev D, Carlsson L, Nattel S. Novel molecular targets for atrial fibrillation therapy. *Nat Rev Drug Discov* 2012;**11**:275–291.
- Neef S, Dybkova N, Sossalla S, Ort KR, Fluschnik N, Neumann K, Seipelt R, Schonhuber FA, Hasenfuss G, Maier LS. CaMKII-dependent diastolic SR Ca<sup>2+</sup> leak and elevated diastolic Ca<sup>2+</sup> levels in right atrial myocardium of patients with atrial fibrillation. *Circ Res* 2010;**106**:1134–1144.
- Voigt N, Li N, Wang Q, Wang W, Trafford AW, Abu-Taha I, Sun Q, Wieland T, Ravens U, Nattel S, Wehrens XH, Dobrev D. Enhanced sarcoplasmic reticulum Ca<sup>2+</sup> leak and increased Na<sup>+</sup>-Ca<sup>2+</sup> exchanger function underlie delayed afterdepolarizations in patients with chronic atrial fibrillation. *Circulation* 2012;**125**:2059–2070.
- Hove-Madsen L, Llach A, Bayes-Genis A, Roura S, Rodriguez FE, Aris A, Cinca J. Atrial fibrillation is associated with increased spontaneous calcium release from the sarcoplasmic reticulum in human atrial myocytes. *Circulation* 2004;**110**:1358–1363.
- Ohkusa T, Ueyama T, Yamada J, Yano M, Fujimura Y, Esato K, Matsuzaki M. Alterations in cardiac sarcoplasmic reticulum Ca<sup>2+</sup> regulatory proteins in the atrial tissue of patients with chronic atrial fibrillation. *J Am Coll Cardiol* 1999;**34**:255–263.
- Zhao ZH, Zhang HC, Xu Y, Zhang P, Li XB, Liu YS, Guo JH. Inositol-1,4,5-trisphosphate and ryanodine-dependent Ca<sup>2+</sup> signaling in a chronic dog model of atrial fibrillation. *Cardiology* 2007;**107**:269–276.
- Lenaerts I, Bito V, Heinzel FR, Driesen RB, Holemans P, D'hooge J, Heidbuchel H, Sipido KR, Willems R. Ultrastructural and functional remodeling of the coupling between Ca<sup>2+</sup> influx and sarcoplasmic reticulum Ca<sup>2+</sup> release in right atrial myocytes from experimental persistent atrial fibrillation. *Circ Res* 2009;**105**:876–885.
- Hell SW, Wichmann J. Breaking the diffraction resolution limit by stimulated emission: stimulated-emission-depletion fluorescence microscopy. *Opt Lett* 1994;**19**:780–782.
- Izu LT, Means SA, Shadid JN, Chen-Izu Y, Balke CW. Interplay of ryanodine receptor distribution and calcium dynamics. *Biophys J* 2006;**91**:95–112.
- Soeller C, Baddeley D. Super-resolution imaging of EC coupling protein distribution in the heart. *J Mol Cell Cardiol* 2013;**58**:32–40.
- Baddeley D, Jayasinghe ID, Lam L, Rossberger S, Cannell MB, Soeller C. Optical single-channel resolution imaging of the ryanodine receptor distribution in rat cardiac myocytes. *Proc Natl Acad Sci USA* 2009;**106**:22275–22280.
- Hou Y, Jayasinghe I, Crossman DJ, Baddeley D, Soeller C. Nanoscale analysis of ryanodine receptor clusters in dyadic couplings of rat cardiac myocytes. *J Mol Cell Cardiol* 2015;**80**:45–55.
- Franzini-Armstrong C, Protasi F, Ramesh V. Shape, size, and distribution of Ca(2+) release units and couplons in skeletal and cardiac muscles. *Biophys J* 1999;**77**:1528–1539.
- Cheng H, Lederer WJ. Calcium sparks. *Physiol Rev* 2008;**88**:1491–1545.
- Dibb KM, Clarke JD, Horn MA, Richards MA, Graham HK, Eisner DA, Trafford AW. Characterization of an extensive transverse tubular network in sheep atrial myocytes and its depletion in heart failure. *Circ Heart Fail* 2009;**2**:482–489.
- Sobie EA, Guatimosim S, Gomez-Viquez L, Song LS, Hartmann H, Saleet JM, Lederer WJ. The Ca<sup>2+</sup> leak paradox and rogue ryanodine receptors: SR Ca<sup>2+</sup> efflux theory and practice. *Prog Biophys Mol Biol* 2006;**90**:172–185.
- MacQuaide N, Ramay HR, Sobie EA, Smith GL. Differential sensitivity of Ca(2+) wave and Ca(2+) spark events to ruthenium red in isolated permeabilised rabbit cardiomyocytes. *J Physiol* 2010;**588**:4731–4742.
- Anne W, Willems R, Holemans P, Beckers F, Roskams T, Lenaerts I, Ector H, Heidbuchel H. Self-terminating AF depends on electrical remodeling while persistent AF depends on additional structural changes in a rapid atrially paced sheep model. *J Mol Cell Cardiol* 2007;**43**:148–158.
- Dedecker P, Muls B, Hofkens J, Enderlein J, Hotta J. Orientational effects in the excitation and de-excitation of single molecules interacting with donut-mode laser beams. *Opt Express* 2007;**15**:3372–3383.
- Cheng H, Song LS, Shirokova N, Gonzalez A, Lakatta EG, Rios E, Stern MD. Amplitude distribution of calcium sparks in confocal images: theory and studies with an automatic detection method. *Biophys J* 1999;**76**:606–617.
- Williams GS, Chikando AC, Tuan HT, Sobie EA, Lederer WJ, Jafri MS. Dynamics of calcium sparks and calcium leak in the heart. *Biophys J* 2011;**101**:1287–1296.
- Marx SO, Gaburjakova J, Gaburjakova M, Henrikson C, Ondrias K, Marks AR. Coupled gating between cardiac calcium release channels (ryanodine receptors). *Circ Res* 2001;**88**:1151–1158.
- Chen W, Wasserstrom JA, Shiferaw Y. Role of coupled gating between cardiac ryanodine receptors in the genesis of triggered arrhythmias. *Am J Physiol Heart Circ Physiol* 2009;**297**:H171–H180.
- Chen-Izu Y, Ward CW, Stark W Jr, Banyasz T, Sumandea MP, Balke CW, Izu LT, Wehrens XH. Phosphorylation of RyR2 and shortening of RyR2 cluster spacing in spontaneously hypertensive rat with heart failure. *Am J Physiol Heart Circ Physiol* 2007;**293**:H2409–H2417.
- Sobie EA, Dilly KW, dos Santos CJ, Lederer WJ, Jafri MS. Termination of cardiac Ca(2+) sparks: an investigative mathematical model of calcium-induced calcium release. *Biophys J* 2002;**83**:59–78.
- Wagner E, Lauterbach MA, Kohl T, Westphal V, Williams GS, Steinbrecher JH, Streich JH, Korff B, Tuan HT, Hagen B, Luther S, Hasenfuss G, Parltz U, Jafri MS, Hell SW, Lederer WJ, Lehnart SE. Stimulated emission depletion live-cell super-resolution imaging shows proliferative remodeling of T-tubule membrane structures after myocardial infarction. *Circ Res* 2012;**111**:402–414.
- Shkryl VM, Blatter LA, Rios E. Properties of Ca<sup>2+</sup> sparks revealed by four-dimensional confocal imaging of cardiac muscle. *J Gen Physiol* 2012;**139**:189–207.
- Soeller C, Crossman D, Gilbert R, Cannell MB. Analysis of ryanodine receptor clusters in rat and human cardiac myocytes. *Proc Natl Acad Sci USA* 2007;**104**:14958–14963.
- Caldwell JL, Smith CE, Taylor RF, Kitmitto A, Eisner DA, Dibb KM, Trafford AW. Dependence of cardiac transverse tubules on the BAR domain protein Amphiphysin II (BIN-1). *Circ Res* 2014;**115**:986–996.
- Landstrom AP, Kellen CA, Dixit SS, van Oort RJ, Garbino A, Weisleder N, Ma J, Wehrens XH, Ackerman MJ. Junctophilin-2 expression silencing causes cardiocyte hypertrophy and abnormal intracellular calcium-handling. *Circ Heart Fail* 2011;**4**:214–223.
- Takekuma H, Komazaki S, Nishi M, Iino M, Kangawa K. Junctophilins: a novel family of junctional membrane complex proteins. *Mol Cell* 2000;**6**:11–22.
- Beavers DL, Wang W, Ather S, Voigt N, Garbino A, Dixit SS, Landstrom AP, Li N, Wang Q, Olivetto I, Dobrev D, Ackerman MJ, Wehrens XH. Mutation E169K in junctophilin-2 causes atrial fibrillation due to impaired RyR2 stabilization. *J Am Coll Cardiol* 2013;**62**:2010–2019.
- Knollmann B, Chopra N, Hlaing T, Akin B, Yang T, Etensohn K, Knollmann BEC, Horton KD, Weissman NJ, Holinstat I, Zhang W, Roden DM, Jones LR, Franzini-Armstrong C, Pfeifer K. Casq2 deletion causes sarcoplasmic reticulum volume increase, premature Ca<sup>2+</sup> release, and catecholaminergic polymorphic ventricular tachycardia. *J Clin Invest* 2006;**116**:2510–2520.
- Swift F, Franzini-Armstrong C, Oyehaug L, Enger UH, Andersson KB, Christensen G, Sejersted OM, Louch WE. Extreme sarcoplasmic reticulum volume loss and compensatory T-tubule remodeling after Serca2 knockout. *Proc Natl Acad Sci USA* 2012;**109**:3997–4001.
- Picht E, Zima AV, Shannon TR, Duncan AM, Blatter LA, Bers DM. Dynamic calcium movement inside cardiac sarcoplasmic reticulum during release. *Circ Res* 2011;**108**:847–856.
- MacQuaide N, Dempster J, Smith GL. Measurement and modeling of Ca<sup>2+</sup> waves in isolated rabbit ventricular cardiomyocytes. *Biophys J* 2007;**93**:2581–2595.
- Cheng H, Lederer WJ, Cannell MB. Calcium sparks: elementary events underlying excitation-contraction coupling in heart muscle. *Science* 1993;**262**:740–744.
- Parker I, Wier WG. Variability in frequency and characteristics of Ca<sup>2+</sup> sparks at different release sites in rat ventricular myocytes. *J Physiol* 1997;**505**(Pt 2):337–344.
- Wang SQ, Song LS, Xu L, Meissner G, Lakatta EG, Rios E, Stern MD, Cheng H. Thermodynamically irreversible gating of ryanodine receptors in situ revealed by stereotyped duration of release in Ca(2+) sparks. *Biophys J* 2002;**83**:242–251.
- Gillespie D, Fill M. Pernicious attrition and inter-RyR2 CICR current control in cardiac muscle. *J Mol Cell Cardiol* 2013;**58**:53–58.
- Zima AV, Bovo E, Bers DM, Blatter LA. Ca(2+) spark-dependent and -independent sarcoplasmic reticulum Ca(2+) leak in normal and failing rabbit ventricular myocytes. *J Physiol* 2010;**588**:4743–4757.

44. Louch WE, Hake J, Mork HK, Hougen K, Skrbic B, Ursu D, Tonnessen T, Sjaastad I, Sejersted OM. Slow Ca(2)(+) sparks de-synchronize Ca(2)(+) release in failing cardiomyocytes: evidence for altered configuration of Ca(2)(+) release units? *J Mol Cell Cardiol* 2013;**58**:41–52.
45. Vest JA, Wehrens XH, Reiken SR, Lehnart SE, Dobrev D, Chandra P, Danilo P, Ravens U, Rosen MR, Marks AR. Defective cardiac ryanodine receptor regulation during atrial fibrillation. *Circulation* 2005;**111**:2025–2032.
46. Terentyev D, Gyorke I, Belevych AE, Terentyeva R, Sridhar A, Nishijima Y, de Blanco EC, Khanna S, Sen CK, Cardounel AJ, Carnes CA, Gyorke S. Redox modification of ryanodine receptors contributes to sarcoplasmic reticulum Ca<sup>2+</sup> leak in chronic heart failure. *Circ Res* 2008;**103**:1466–1472.
47. Gonzalez DR, Treuer AV, Castellanos J, Dulce RA, Hare JM. Impaired S-nitrosylation of the ryanodine receptor caused by xanthine oxidase activity contributes to calcium leak in heart failure. *J Biol Chem* 2010;**285**:28938–28945.
48. Yamazaki M, Vaquero LM, Hou L, Campbell K, Zlochiver S, Klos M, Mironov S, Berenfeld O, Honjo H, Kodama I, Jalife J, Kalifa J. Mechanisms of stretch-induced atrial fibrillation in the presence and the absence of adrenergic stimulation: interplay between rotors and focal discharges. *Heart Rhythm* 2009;**6**:1009–1017.
49. Bhuiyan ZA, van den Berg MP, van Tintelen JP, Bink-Boelkens MT, Wiesfeld AC, Alders M, Postma AV, van Langen I, Mannens MM, Wilde AA. Expanding spectrum of human RYR2-related disease: new electrocardiographic, structural, and genetic features. *Circulation* 2007;**116**:1569–1576.
50. Brochet DX, Xie W, Yang D, Cheng H, Lederer WJ. Quarky calcium release in the heart. *Circ Res* 2011;**108**:210–218.
51. Shirokova N, Kang C, Fernandez-Tenorio M, Wang W, Wang Q, Wehrens XH, Niggli E. Oxidative stress and Ca(2+) release events in mouse cardiomyocytes. *Biophys J* 2014;**107**:2815–2827.
52. Cannell MB, Kong CH, Imtiaz MS, Laver DR. Control of sarcoplasmic reticulum Ca<sup>2+</sup> release by stochastic RyR gating within a 3D model of the cardiac dyad and importance of induction decay for CICR termination. *Biophys J* 2013;**104**:2149–2159.